

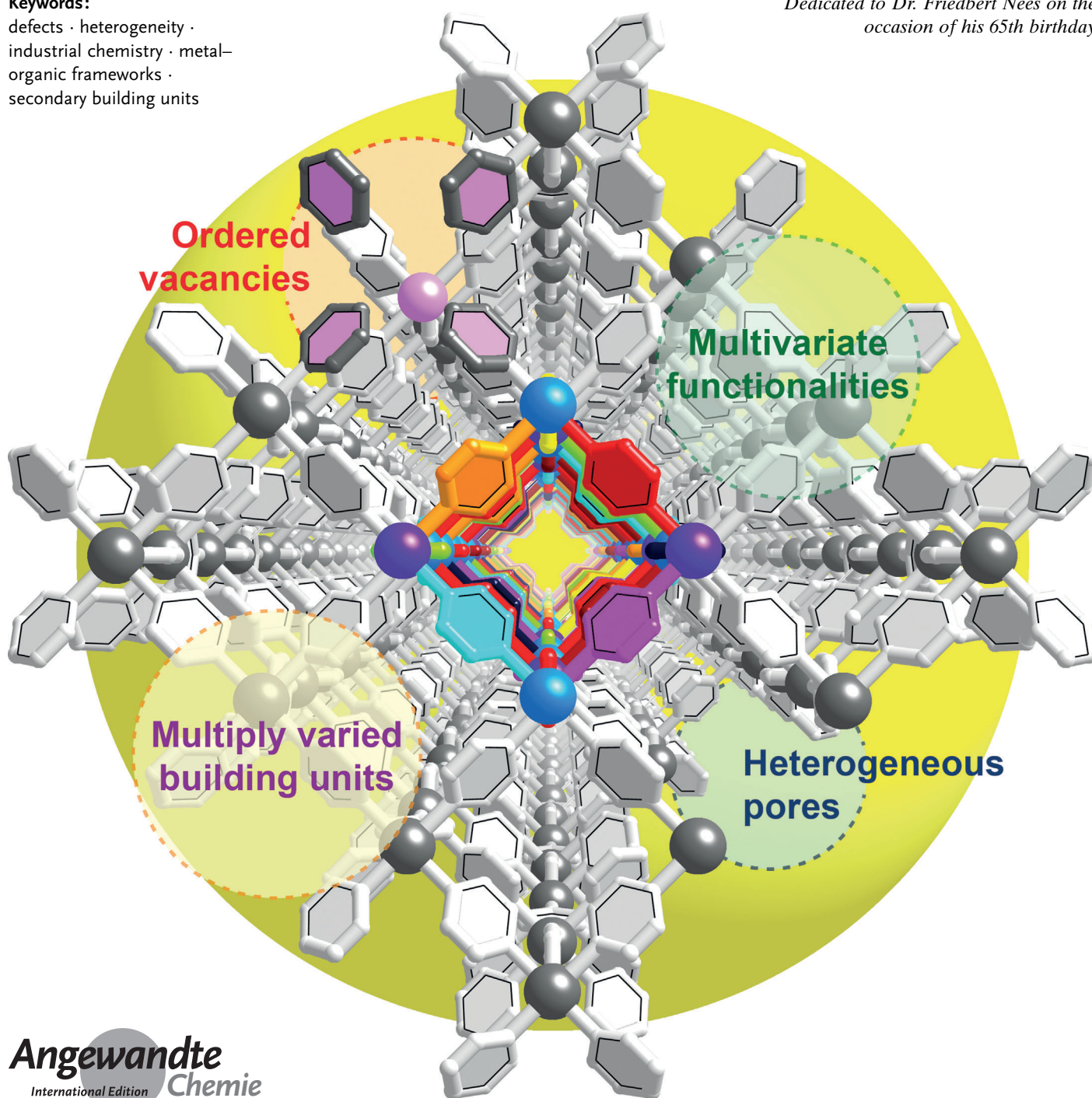
# “Heterogeneity within Order” in Metal–Organic Frameworks

Hiroyasu Furukawa,\* Ulrich Müller,\* and Omar M. Yaghi\*

**Keywords:**

defects · heterogeneity · industrial chemistry · metal–organic frameworks · secondary building units

*Dedicated to Dr. Friedbert Nees on the occasion of his 65th birthday*



**M**etal–organic frameworks (MOFs) are constructed by linking inorganic units with organic linkers to make extended networks. Though more than 20 000 MOF structures have been reported most of these are ordered and largely composed of a limited number of different kinds building units, and very few have multiple different building units (heterogeneous). Although heterogeneity and multiplicity is a fundamental characteristic of biological systems, very few synthetic materials incorporate heterogeneity without losing crystalline order. Thus, the question arises: how do we introduce heterogeneity into MOFs without losing their ordered structure? This Review outlines strategies for varying the building units within both the backbone of the MOF and its pores to produce the heterogeneity that is sought after. The impact this heterogeneity imparts on the properties of a MOF is highlighted. We also provide an update on the MOF industry as part of this themed issue for the 150th anniversary of BASF.

## 1. Introduction

The Irish playwright George Bernard Shaw once wrote: “Some people see things as they are and say, why? I dream things that never were and say, why not?” The latter part describes the spirit of the approach with which metal–organic frameworks (MOFs) were first made as robust carboxylate frameworks with permanent porosity in the 1990s<sup>[1]</sup> and later scaled up by BASF who collaborated with academia on developing the industry of MOFs.<sup>[2]</sup> This spirited collaboration continues to expand and intensify to this day. The ability to control MOFs’ structure, porosity, and properties on the molecular level has led to numerous advances in the basic science of building designed chemical structures. Furthermore, this new level of control has led to fascinating developments with respect to applications in gas storage, separation, and many fields of catalysis.<sup>[3,4]</sup>

Herein, we present a view of MOFs that goes beyond these aspects and explore how we can use the ordered structures of MOFs to create more complex structures and pore environments.<sup>[5]</sup> Heterogeneity in MOFs can be defined as the presence of multiple kinds of building units and/or covalently linked functionalities onto their backbone structure. This definition also encompasses any deviations from perfect order, such as the presence of vacancies, multiple pore sizes (micro, meso, and macro) in an otherwise crystalline system. Indeed, we use the term heterogeneity to describe means of producing more complex MOF structures by design. Scenarios of heterogeneity do exist in inorganic crystals and other systems. The principal difference between the usual inorganic systems of solid solutions and the like and MOFs, is that in a MOF the elements (components) of heterogeneity are covalently linked to the backbone and/or their position is known but their spatial arrangement is not readily identified. Another important aspect pertains to the fact that any heterogeneity attached to a MOF structure is metrically defined as it is superimposed covalently on a well-defined structure.

## From the Contents

1. Introduction	3418
2. Heterogeneity within Order	3419
3. MOFs in Industry: An Update	3427
4. Summary and Outlook	3428

As described below, we seek to answer the question: can we, as chemists, introduce heterogeneity within ordered MOF structures<sup>[6]</sup> in a designed fashion and harness any added benefits that the introduction of such heterogeneity might impart onto the material? It is important that such introduction of heterogeneity maintains the long-range order (crystallinity) of the MOF structure. We note that the arrangement of such heterogeneity in crystals raises the question of how the elements (components) of heterogeneity are arranged in the crystal. Many interesting approaches have been contemplated and some successfully implemented concerning how to determine the spatial arrangement of the elements of heterogeneity in the MOF crystal.<sup>[7,8]</sup> This notion of introducing “heterogeneity within order” can take on many different forms, involving not only the metal–organic backbone of the MOF, but also the interior space of the MOF. More specifically, we describe examples of heterogeneity within order (Figure 1) based on:

- mixing of organic linkers within the MOF backbone,
- mixing of the metal-containing secondary building units (SBUs),
- mixing of both the SBUs and organic linkers within the same MOF backbone,
- mixing of functional groups along the backbone,

[\*] Dr. H. Furukawa, Prof. Dr. O. M. Yaghi  
Department of Chemistry, University of California-Berkeley, Materials Sciences Division, Lawrence Berkeley National Laboratory, and Kavli Energy NanoSciences Institute at Berkeley  
Berkeley, California 94720 (USA)  
(O.M.Y.)  
E-mail: furukawa@berkeley.edu  
yaghi@berkeley.edu  
Dr. H. Furukawa, Prof. Dr. O. M. Yaghi  
King Abdulaziz City of Science and Technology  
P.O. Box 6086, Riyadh 11442 (Saudi Arabia)  
Dr. U. Müller  
BASF SE, Chemicals Research and Engineering  
Ludwigshafen 67056 (Germany)  
E-mail: ulrich.mueller@BASF.com

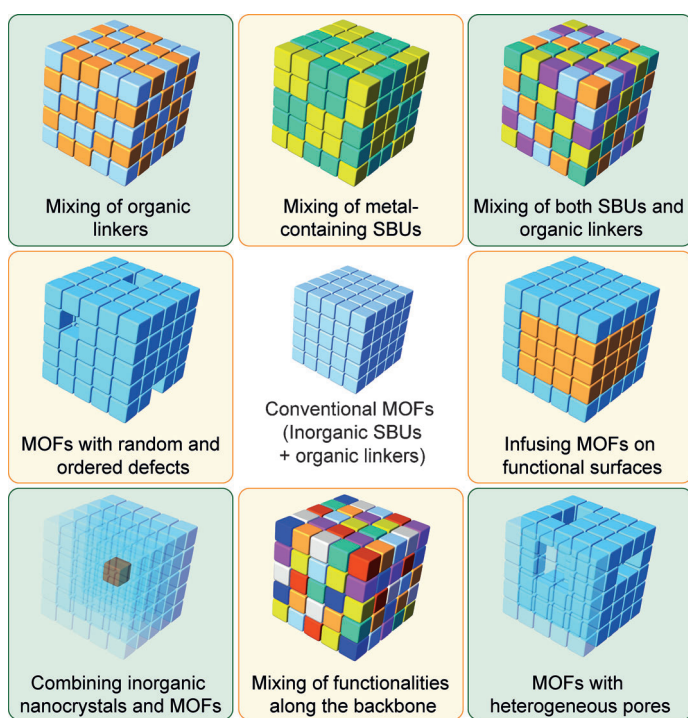


**Figure 1.** Various strategies for introducing “heterogeneity within order” into MOF structures.

- e) MOFs with random and ordered defects,
- f) attaching MOFs to functional surfaces,
- g) combining inorganic nanocrystals and MOFs,
- h) MOFs with heterogeneous pores.

We show how these constructs introduce heterogeneity in MOFs without losing their order, and, where applicable, how the heterogeneity provides opportunities and chemistry that are unobtainable otherwise. Finally, we end with a Section highlighting the state-of-the-art processes of the industrialization of MOFs by BASF, to provide a contextual means for the future development of new MOF materials. On a fundamental level, learning how to deliberately design heterogeneity within order in MOFs and related materials opens a wide range of opportunities to harness new special properties, with which such heterogeneity endows a MOF material.



Hiroyasu Furukawa was born in Chiba (Japan) in 1971. He completed his Ph.D. at University of Tokyo in 2000 with Prof. Tadashi Watanabe. After postdoctoral studies at Waseda University and the National Institute of Advanced Industrial Science and Technology (AIST; Japan), he joined Prof. O. Yaghi's research group in 2003 at University of Michigan. He is currently a Project Scientist at University of California, Berkeley. His research interests include the use of new porous materials for energy-related applications.



Ulrich Müller studied chemistry at Johannes Gutenberg University, Mainz. He received his Ph.D. in the group of Prof. K. K. Unger working on the synthesis of large zeolite crystals and sorption properties. He joined BASF SE in 1989 and currently is Senior Vice President and Executive Expert Zeolite Catalysis since 2011. He has worked on CFC-free polyurethane foams, catalysts for crop protection agents, chemical intermediates, adsorptive olefin purifications, catalysts for epoxidation processes of propylene and catalysts for automotive emission control. He initiated MOF-research at BASF early on and started the joint BASF-CNSI laboratory with Prof. Yaghi at UCLA.

## 2. Heterogeneity within Order

### 2.1. Mixing of More than One Organic Linker within the MOF Backbone

One of the simple ways to introduce heterogeneity into a MOF structure is to utilize more than two types of organic linker. Early reports showed that pillar molecules, such as 1,4-diazabicyclo[2.2.2]octane (DABCO), can be used to bridge two-dimensional (2D) MOF layers to construct three-dimensional (3D) MOF structures. One of the earliest examples was reported in 2001,  $[\text{Cu}_2(\text{BPDC})_2(\text{DABCO})]$  (BPDC = biphenyl-4,4'-dicarboxylate) for high-pressure  $\text{CH}_4$  storage.<sup>[9]</sup> By applying this mixed-linker, pillar strategy, a series of 3D MOF structures were demonstrated using different pillar molecules.<sup>[10]</sup> The topology of these MOFs was typically found to be primitive cubic (**pcu**) because linear ditopic linkers were employed.<sup>[11]</sup>

Through a combination of ditopic and tritopic linkers, it is possible to synthesize more complex topologies. The first example of this type of strategy was reported in 2008, UMCM-1  $[(\text{Zn}_4\text{O})_3(\text{BDC})_4(\text{BTB})_4]$  (BDC = 1,4-benzenedicarboxylate, BTB = 4,4',4''-benzene-1,3,5-triyl-tribenzoate) (Figure 2a).<sup>[12a]</sup> The unique topology (**muo**) of this MOF does not permit the formation of an interpenetrating structure (because it is a heterodual),<sup>[11b]</sup> and thus it is possible to form a highly open MOF. This result is in sharp contrast to the **pcu** net, which is a self-dual.<sup>[10a,d,e,f]</sup> By changing the length of the ditopic and tritopic linkers, it was possible to make even more-porous frameworks, such as UMCM-2  $[(\text{Zn}_4\text{O})_3(\text{T2DC})_3(\text{BTB})_4]$  (T2DC = thieno[3,2-*b*]thiophene-2,5-dicarboxylate) and MOF-210  $[(\text{Zn}_4\text{O})_3(\text{BPDC})_3(\text{BTE})_4]$  (BTE = 4,4',4''-(benzene-1,3,5-triyl-tris(ethylene-2,1-diyl))tribenzoate; Figure 2b).<sup>[12b,13]</sup> Note that MOFs composed of three different carboxylate linkers have also been reported.<sup>[14]</sup> For instance, UMCM-12  $[(\text{Zn}_4\text{O})_2(\text{TPA})_2(\text{BDC})(\text{TMTTPDC})_2]$  (TPA = 4,4',4''-nitrioltribenzoate, TMTTPDC = 2',3',5',6'-tertramethylterphenyl-4,4''-dicarboxylate) contains a tritopic linker and two ditopic linkers of different length (Figure 2c).<sup>[14b]</sup> These materials have some of the highest surface areas and pore volumes reported, highlighting the usefulness of synthesizing MOFs based on a mixed linker strategy.

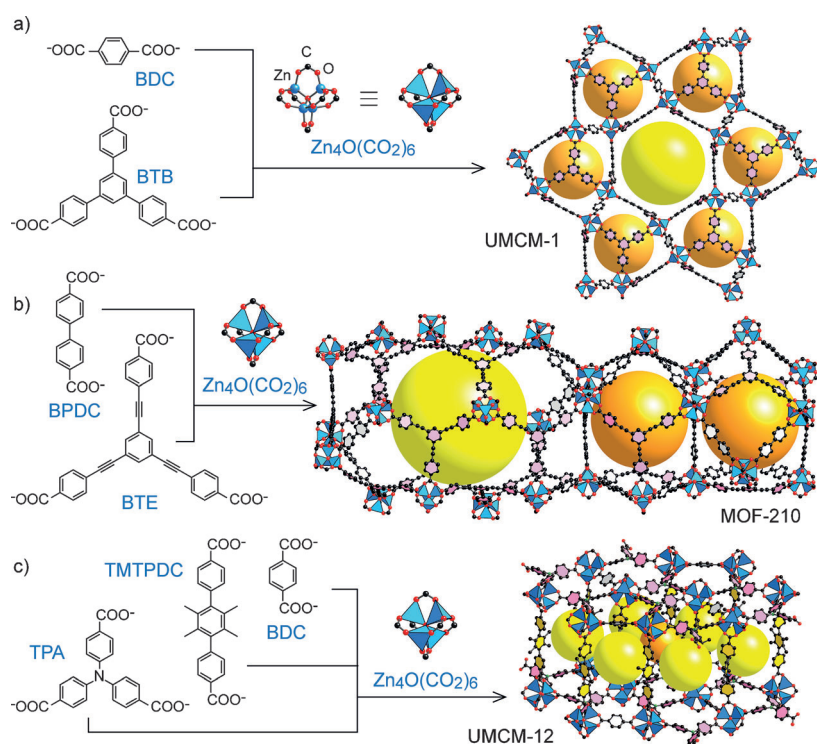


**Figure 2.** UMCM-1 (a), MOF-210 (b), and UMCM-12 (c) are composed of two or three different linkers connected to a  $Zn_4O$  unit. Zn blue polyhedra, O red, C black, all hydrogen atoms are omitted for clarity. The large yellow and orange spheres represent the largest spheres that could occupy the cavity.

It is likely that in a mixed-linker system when the two types of linker have identical shapes, they will be randomly distributed in the framework.<sup>[15]</sup> However, this is not always the case, especially when linkers show preference to specific positions in the crystal structure. The **GME**-type zeolitic imidazolate frameworks (ZIFs) [ $Zn(NO_2\text{-Im})(X\text{-bIm})$ ] (Im = imidazolate, bIm = benzimidazolate, X = H for ZIF-68, Cl for ZIF-69), reported in 2008, serve as a valuable, representative example (Figure 3a).<sup>[15a]</sup> In the **GME** ZIF structure, the position of the nitroimidazolate linker consistently resides within the *hpr* cage, even upon integration of other functionalized imidazolate linkers. As a result, the 1D channel of **GME** ZIFs was decorated with desirable functionalities without changing their underlying topology or having

a random distribution of the linkers throughout the framework. This strategy proved worthwhile when it was applied towards making other topologies, for which functionalized imidazolate linkers (bIm, Cl-bIm, Me-bIm, Br-bIm,  $NO_2\text{-bIm}$ , and CN-Im) were introduced within the resulting ZIFs' pores.<sup>[16]</sup> More importantly, gas adsorption measurements of **GME** ZIFs showed that  $CO_2$  selectivity was tuned by changing the incorporated functionalities; ZIFs constructed from a polar functionalized linker ( $NO_2\text{-bIm}$  for ZIF-78, and CN-Im for ZIF-82) exhibited higher  $CO_2$  selectivities over  $CH_4$ ,  $N_2$ , and  $O_2$  than nonpolar functionalized linkers ( $CH_3\text{-bIm}$  for ZIF-79).

The **CHA**-type ZIFs [ $Zn(CH_3\text{-Im})_x(X\text{-bIm})_{(2-x)}$ ] (X = Br, Cl, and  $CH_3$  for ZIF-300, 301, and 302, respectively) also containing *hpr* cages demonstrate a similar trend;  $CH_3\text{-Im}$  linkers were always found in the same position with the *hpr* cage (Figure 3b).<sup>[17]</sup> This discovery implied that the formation of the *hpr* cage could direct the overall structure of new ZIF materials. Owing to the nonpolar functionalities (i.e. Br, Cl, and  $CH_3$ ), the pores of these **CHA** ZIFs were extremely hydrophobic as confirmed by water adsorption isotherms. Such hydrophobic pores enable the ZIFs to selectively capture  $CO_2$  from a flow of binary gas mixture containing  $CO_2$  and wet (80% relative humidity of water)  $N_2$ .

## 2.2. Mixing of More than One Metal-Containing SBU

MOFs having different types of inorganic secondary building unit (SBU) have been prepared by employing two types of metal ion during the synthesis.<sup>[18]</sup> For example, when a series of lanthanide metals (Ln = Pr, Gd, and Er) were treated with a Mn salt source and pyridine-2,6-dicarboxylic acid ( $H_2DIPIC$ ), the resulting MOFs [ $Ln(DIPIC)_3Mn_{1.5}(H_2O)_3$ ] showed enneatopic and tritopic metal SBUs.<sup>[19]</sup> Similarly, by employing In and Zr metals, a mixed-coordination metal-imidazolate framework, ZIF-5 [ $In_2Zn_3(Im)_{12}$ ] was obtained, where  $Zn^{2+}$  and  $In^{3+}$  are in tetrahedral and octahedral coordination geometries, respectively.<sup>[20]</sup>

One of the first examples of a MOF constructed from a single metal ion, yet containing different SBUs, was reported in 2005, USF-4 [ $Zn_6(BTC)_4(\text{isoquinoline})_4(\text{MeOH})_2$ ] (BTC = benzene-1,3,5-tricarboxylate).<sup>[21]</sup> In this structure, tritopic BTC linkers were connected with dinuclear square and tetrahedral inorganic Zn SBUs. Two types of inorganic SBU were also introduced through the use of a tritopic linker (biphenyl-3,4',5-tricarboxylate, BPTC): UMCM-150 [ $Cu_3(BPTC)_2$ ] is composed of Cu paddle-wheel and trinuclear trigonal-prism Cu SBUs.<sup>[22]</sup> The resulting material has a high Langmuir surface area ( $3100\text{ m}^2\text{ g}^{-1}$ ) and excess  $H_2$  uptake capacity (5.4 wt% at 77 K and 45 bar). More



Omar M. Yaghi received his Ph.D. from the University of Illinois-Urbana (1990) with Prof. Walter G. Klemperer, and studied as a postdoctoral fellow at Harvard University with Prof. Richard Holm. He is currently the James and Neeltje Tretter Professor of Chemistry, University of California, Berkeley, and Faculty Scientist at Lawrence Berkeley National Laboratory. His research has shown that organic and inorganic molecules can be stitched together by covalent bonds to make extended porous structures, such as MOFs, ZIFs, and COFs.

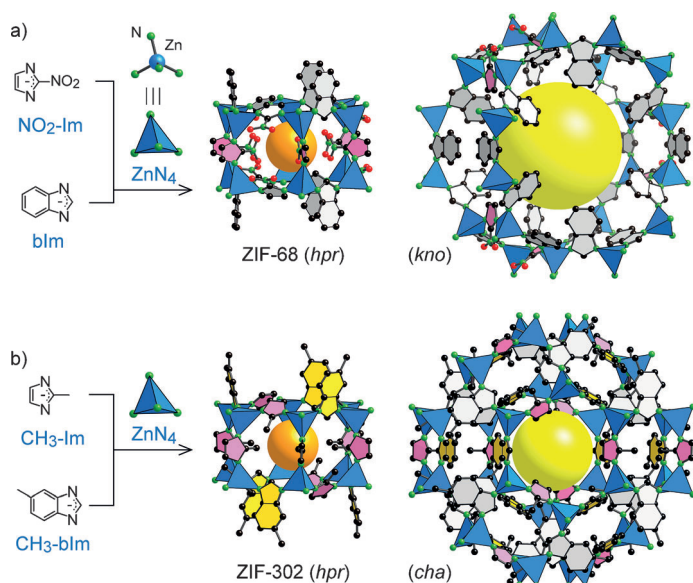


**Figure 3.** Reaction of two imidazolate linkers with zinc(II) ions resulting in ZIF-68 (a) and ZIF-302 (b). Light red imidazole and gray benzimidazole linkers are found in specific positions, while yellow benzimidazole linkers can be replaced with Me-Im linkers. Zn blue polyhedra, N green, O red, C black; all hydrogen atoms are omitted for clarity.

recently, a hexatopic linker with four, three-coordinated branching points [trimethyl substituted 3,3',3'',5,5',5''-benzene-1,3,5-triylhexabenzate (TMBHB)] was employed to obtain a **tfe-b** net possessing dinuclear triangular and square SBUs,  $[\text{Zn}_7(\text{TMBHB})_2(\text{NO}_3)_2]$  (Figure 4a).<sup>[23]</sup> Another approach for designing MOFs with two kinds of inorganic SBU involves the utilization of organic linkers with two

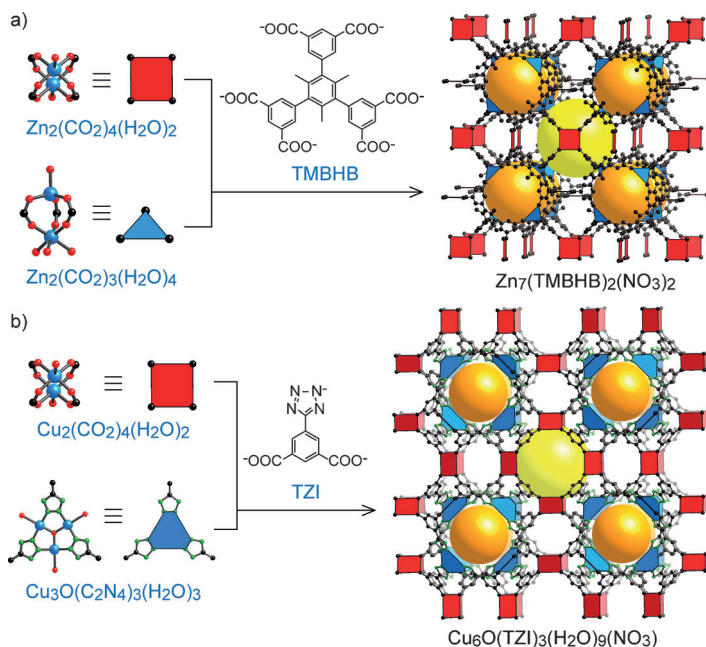


**Figure 4.** Two types of inorganic SBU are used to obtain 3D MOF structures: a)  $[\text{Zn}_7(\text{TMBHB})_2(\text{NO}_3)_2]$  and b)  $[\text{Cu}_6\text{O}(\text{TZI})_3(\text{H}_2\text{O})_9(\text{NO}_3)]$ . Square and triangle SBUs are shown in red and blue, respectively.

different terminal functional groups, such as 5-tetrazolyl-isophthalic acid ( $\text{H}_3\text{TZI}$ ).<sup>[24]</sup> In this case, carboxylate terminals of TZI linker form metal–organic polyhedron-1 (MOP-1,  $[\text{Cu}_{24}(\text{mBDC})_{24}]$ ;  $\text{mBDC}$  = isophthalate)<sup>[25]</sup> like cages with Cu paddle-wheels, which are connected through terminal tetrazole units  $[\text{Cu}_3\text{O}_4(\text{-CN}_4)_3]$  (Figure 4b). Overall, the structure can be described as a (3,24)-connected **rh**t net  $[\text{Cu}_6\text{O}(\text{TZI})_3(\text{H}_2\text{O})_9(\text{NO}_3)]$ .

### 2.3. Mixing Multiple Inorganic SBUs and More than One Organic Linker within the Same MOF

By employing more than two types of organic and/or inorganic SBU, a more complex framework was obtained in one-pot reactions. In 2011, a MOF having a cage-within-cage structure, CPM-24  $\{[\text{Co}_9(\text{OH})_2(\text{acetate})\text{-}(\text{BTC})_4(\text{IN})_8(\text{H}_2\text{O})_2][(\text{CH}_3)_2\text{NH}_2]_5$  ( $\text{IN}$  = isonicotinate), was reported (Figure 5);<sup>[26]</sup> each larger rhombicuboctahedral cage, composed of Co binuclear units  $[\text{Co}_{48}(\text{IN})_{48}]$ , contains smaller cuboctahedral cages with Co paddle-wheel and BTC linkers  $[\text{Co}_{24}(\text{BTC})_{24}]$  (Figure 5b). Furthermore,  $\text{IN}$  is coordinated to the outer surface of the Co paddle-wheels, in which four of these  $\text{IN}$  form another Co paddle-wheel unit (Figure 5c). CPM-24 showed high  $\text{CO}_2$  uptake capacity ( $68.4 \text{ cm}^3 \text{ g}^{-1}$  at 1 atm and 273 K), but negligible  $\text{N}_2$  uptake under the same conditions; therefore, high  $\text{CO}_2/\text{N}_2$  selective adsorption was expected (calculated  $\text{CO}_2/\text{N}_2$  selectivity = 106:1 at 0.16 atm).

To design desirable structures with many types of organic linkers and metal ions, molecular building blocks can be assembled through two-step reactions (Figure 6).<sup>[27]</sup> In this example, in the first step, Cr trigonal prism SBUs  $\{[\text{Cr}_3\text{O}(\text{H-IN})_4(\text{IN})_2(\text{H}_2\text{O})_3](\text{NO}_3)_3\}$  were prepared. Since the terminal sites of these Cr SBUs were decorated with pyridine units, the building blocks were easily bound to  $\text{Zn}^{2+}$  ions and tritopic organic linkers to form  $\{\text{Zn}_3\text{-}(\text{BTC})_2[\text{Cr}_3\text{O}(\text{IN})_6(\text{H}_2\text{O})_2(\text{OH})]\}$  (tp-PMBB-1-**asc**-1). Expanded derivatives of tritodal MOFs (i.e. containing triangular, tetrahedral, and trigonal prismatic SBUs) were also obtained by employing larger tritopic organic linkers.<sup>[27]</sup> The presence of permanent microporosity for tp-PMBB-1-**asc**-1 was demonstrated by  $\text{N}_2$  isotherm measurements on the guest-free form of the material (BET surface area =  $1671 \text{ m}^2 \text{ g}^{-1}$ ). This material also showed enhanced  $\text{CO}_2$  uptake capacity ( $136 \text{ cm}^3 \text{ g}^{-1}$  at 1 atm and 273 K compared to that of CPM-24).<sup>[26]</sup>

### 2.4. Mixing of Multiple Functional Groups along the Backbone

Another strategy for designing heterogeneity within MOFs is to incorporate two or more types of functionality in a MOF framework. The challenge presented is how to mix two or more organic linkers of the same type, each having unique functionality, without producing mixed phases rather than a single, pure MOF phase with varying functionalities. In 2010, multivariate MOFs

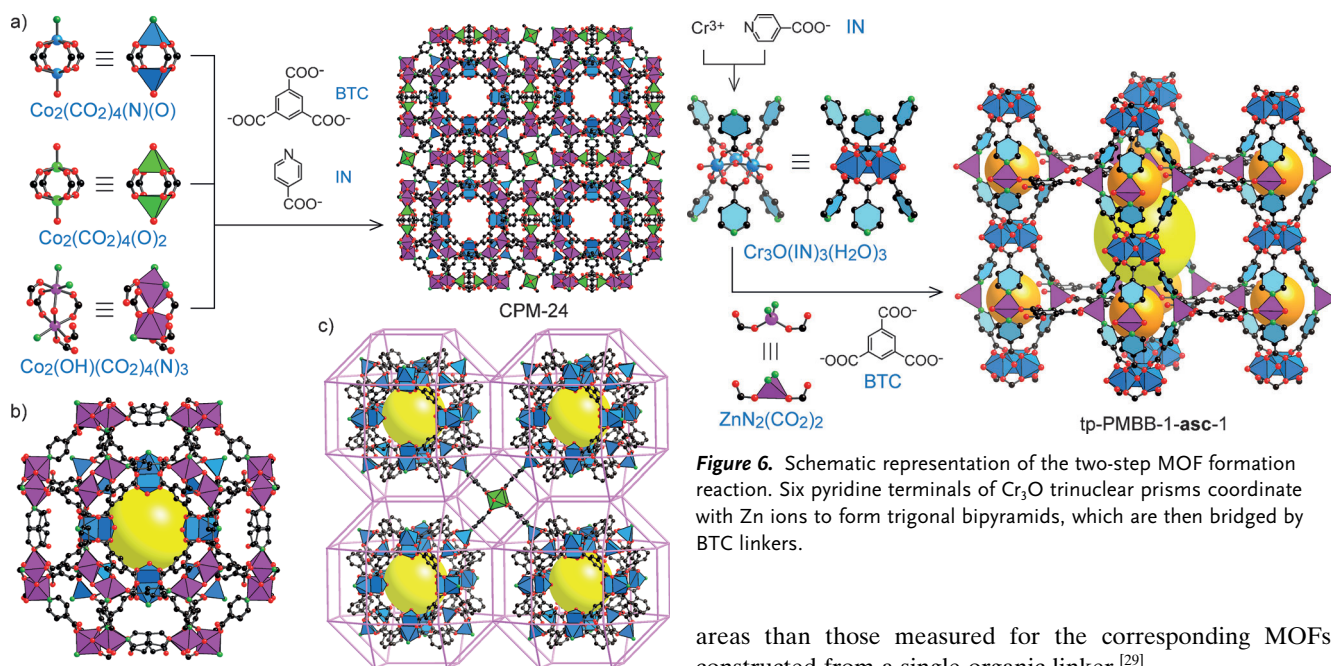
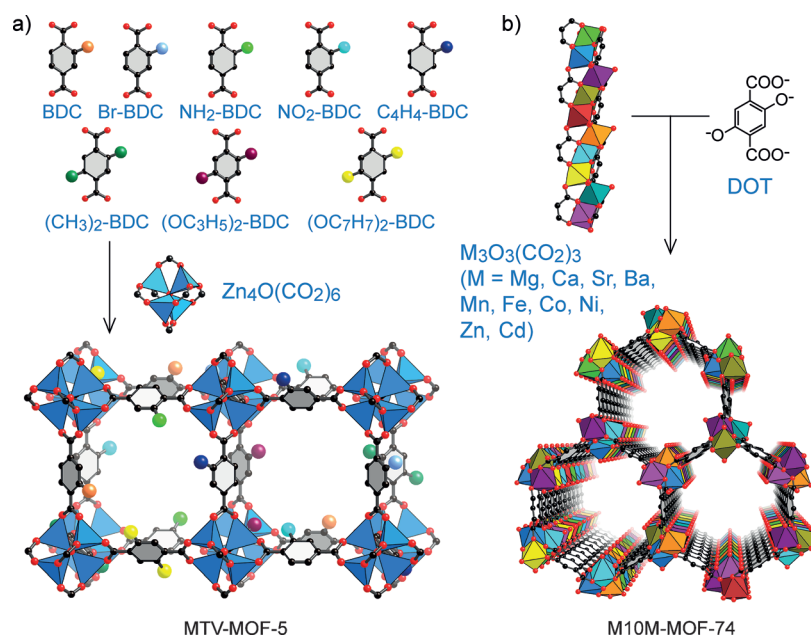


**Figure 5.** Cobalt paddle-wheel (blue and green) and hydroxy bridged cobalt dinuclear (purple) SBUs are connected with BTC and IN linkers to form CPM-24 (a). Small MOP cages (blue) are found in larger rhombicuboctahedral cages (purple) (b), and 4 MOP cages are connected with paddle-wheel units shown in green (c). Large polyhedra represented by the pink outline show the  $\text{Co}_{48}(\text{IN})_{48}$  cages.

(MTV-MOFs), where multiple organic functionalities were incorporated into a MOF-5 [ $\text{Zn}_4\text{O}(\text{BDC})_3$ ]<sup>[28]</sup> structure, were reported.<sup>[7]</sup> One of the MTV-MOF-5 materials contains eight different functionalized BDC linkers (X-BDC, X = H,  $\text{NH}_2$ , Br,  $\text{NO}_2$ ,  $(\text{CH}_3)_2$ ,  $\text{C}_4\text{H}_4$ ,  $(\text{OC}_3\text{H}_5)_2$ , and  $(\text{OC}_7\text{H}_7)_2$ ) within its structure without losing either the parent MOF-5 backbone structure, crystallinity, or microporosity (Figure 7 a). The arrangement of organic linkers in the MOF structure was not fully elucidated; however, through solid-state NMR spectral analysis as well as molecular dynamics simulations, an apportionment of organic functionalities within the MTV-MOF structure was found depending on the type of functionality used. For example, it was observed that  $-\text{NH}_2$  and  $(-\text{CH}_3)_2$  functionalized linkers tended to form small clusters within the MTV-MOF, whereas  $-\text{NO}_2$ ,  $(-\text{OC}_3\text{H}_5)_2$ , and  $(-\text{OC}_7\text{H}_7)_2$  functionalized linkers were well-mixed throughout the framework.<sup>[8]</sup> The MTV material had an  $\text{CO}_2$  uptake capacity improved by 400 % compared to the parent MOF-5 architecture, and this trend was reproduced through simulation calculations.<sup>[7]</sup> The plausible explanation for this observed high  $\text{CO}_2$  affinity is that MTV materials have both large numbers of adsorption sites and sufficient pore space. Such nonlinear properties are also reported for MTV compounds, which show higher surface

areas than those measured for the corresponding MOFs constructed from a single organic linker.<sup>[29]</sup>

In contrast to MTV-MOFs containing various kinds of organic functionalities, the history of MOFs containing two or more different metal ions is more extensive. In 1992,  $\text{N}(\text{C}_4\text{H}_9)_4[\text{MCr}(\text{oxalate})_3]$  ( $\text{M} = \text{Mn}^{2+}$ ,  $\text{Fe}^{2+}$ ,  $\text{Co}^{2+}$ ,  $\text{Ni}^{2+}$ ,  $\text{Cu}^{2+}$ ,  $\text{Zn}^{2+}$ ) type structures were synthesized by a one-pot reaction.<sup>[30]</sup> These materials have magnetic features characteristic of ferromagnets; however, their porous nature was not studied, perhaps because of the presence of bulky  $\text{NBU}_4$  counter cations in the framework. Recently, it was reported that Co-doped MOF-5 structures could be prepared through a one-pot synthesis, in which 8 % or 21 % of  $\text{Zn}^{2+}$  ions were



replaced with  $\text{Co}^{2+}$  ions, respectively.<sup>[31]</sup> From the detailed analysis of these materials, it is presumed that  $\text{Co}^{2+}$  ions were incorporated into the framework; however, the precise location of these doped metal ions was not clear. Even more recently, a microcrystalline MOF-74 [ $\text{Zn}_2(\text{DOT})$ ] (DOT = dioxidoterephthalate)<sup>[32]</sup> structure was obtained, through a one-pot reaction, containing up to 10 different kinds of divalent metals (Mg, Ca, Sr, Ba, Mn, Fe, Co, Ni, Zn, and Cd) within the structure (Figure 7b).<sup>[33]</sup> The distribution of metal ions in the crystalline powder samples was studied by energy-dispersive X-ray spectroscopy, which indicated that the distribution of the metal ions might not be uniform.

Mixed-metal MOFs were also obtained by post-synthetic metal exchange reactions. For instance, 98% of  $\text{Cd}^{2+}$  ions in a Cd-MOF  $\{\text{Cd}_{1.5}(\text{H}_3\text{O})_3[(\text{Cd}_4\text{O})_3(\text{HETT})_8]\cdot 6\text{H}_2\text{O}\}$  ( $\text{H}_3\text{HETT} = 5,5',10,10',15,15'$ -hexaethyltruxene-2,7,12-tricarboxylic acid) were replaced by  $\text{Pb}^{2+}$  ions through immersing the MOF in a  $\text{Pb}(\text{NO}_3)_2$  solution.<sup>[34]</sup> Single-crystal X-ray diffraction analyses of these materials revealed that the M–O (M = Cd and Pb) distances are different from one another, thus making it reasonable to conclude that the ion-exchange process occurred without loss of the material's crystallinity.  $\text{Zn}^{\text{II}}$  ions in MOF-5 have also been exchanged with metal ions ((Cl)Ti<sup>III</sup>, V<sup>II</sup>, (Cl)V<sup>III</sup>, Cr<sup>II</sup>, Mn<sup>II</sup>, or Fe<sup>II</sup>) that could not otherwise be incorporated into the framework through a direct synthesis route.<sup>[35]</sup> It could be shown that when the metal ions were introduced into the MOF-5 framework with reduced oxidation states, they could be subsequently oxidized without changing the framework structure (transformation from Cr<sup>II</sup>-MOF-5 to  $(\text{BF}_4)\text{Cr}$ -MOF-5 by exposure to  $\text{NOBF}_4$  in acetonitrile).

### 2.5. MOFs with Random and Ordered Defects

Introduction of defect sites into ordered structures is also a useful strategy to realize unusual heterogeneous structures and properties, even if it is a big challenge to elucidate how the defect sites are distributed in the framework.<sup>[36]</sup> One of the easiest methods to introduce such sites is by post-synthetic acid treatment.<sup>[37]</sup> Brønsted acid sites have been introduced into MIL-100(Fe) [ $\text{Fe}_3\text{O}(\text{H}_2\text{O})_3(\text{BTC})_2$ ], without structural or porosity damage, by immersing the material in an aqueous solution of  $\text{CF}_3\text{COOH}$  or  $\text{HClO}_4$ . Although the local structure is unclear, it is likely that extra open metal sites were created by the acid treatment.<sup>[37,38]</sup>

Another method for incorporating defects is to utilize modulator molecules, such as acetic acid and formic acid.<sup>[39,40]</sup> When modulator molecules are added during the MOF synthesis, they can be incorporated into the framework to create heterogeneity (as a result of missing organic linkers) even after sample activation. Through the addition of trifluoroacetic acid (TFA) within the appropriate reaction mixture to synthesize UiO-66 [ $\text{Zr}_6\text{O}_4(\text{OH})_4(\text{BDC})_6$ ], it was found that some of the BDC linkers were replaced with trifluoroacetate.<sup>[39]</sup> The resulting structure showed enhanced catalytic activity in the cyclization of citronellal to isopulegol. The presence of defects was also confirmed by x-ray diffraction measurements.<sup>[40]</sup>

The third strategy for introducing this type of heterogeneity is by rapid precipitation of MOF.<sup>[41]</sup> Although conventional solvothermal synthesis requires anywhere from 12 h to several days to yield single crystal samples, it is expected that defect sites within a MOF structure will result unavoidably from fast crystal formation (< 1 min).<sup>[42]</sup> To investigate whether Brønsted -OH groups (Zn-OH species) can be introduced, MOF-5 was prepared by a room-temperature synthesis with and without 2-methyltoluic acid (modulator).<sup>[41]</sup> Fourier-transform infrared (FT-IR) data implied the presence of -OH functionalities; however, considering the products low crystallinity and surface area, it may be likely that the Zn-OH moiety was not introduced into the MOF-5 structure.

Perhaps the most common strategy in the creation of defect sites is by co-assembly of metal ion, linker, and fragment of the parent linker.<sup>[36,43,44]</sup> One of the early examples reported was PCN-125 [ $\text{Cu}_2(\text{TPTC})$ ] (TPTC = 1,1':4,1''-terphenyl-3,3'',5,5''-tetracarboxylate), which is composed of Cu paddle-wheel units connected by tetratopic TPTC linkers.<sup>[45]</sup> Since *m*BDC is a fragment of the TPTC linker in PCN-125, functionalized R-*m*BDC (R = H,  $\text{CH}_3$ ,  $\text{NH}_2$ ,  $\text{NO}_2$ ,  $\text{CH}_2\text{NH}_2$ ,  $\text{SO}_3\text{Na}$ ,  $\text{SO}_3\text{H}$ , or  $\text{CH}_2\text{N}_3$ ) linkers were added to the reaction mixture used to synthesize PCN-125. Such MOF materials displayed identical powder X-ray diffraction patterns to the original PCN-125 and solution-state NMR analyses (based on digested MOF samples) confirmed the presence of R-*m*BDC linkers within the structures. This synthetic approach was in sharp contrast to those of other mixed-linker systems, such as UMCM-1 and MOF-210, which yield MOFs with complex topologies.<sup>[12,13]</sup> It is noted that the pore diameters of several of these defective MOFs increased when shorter linkers were incorporated. In effect, this strategy can enable both pore expansion and functionalization. Indeed, several of these MOFs containing linker fragments showed improved  $\text{CO}_2$  uptake when compared to the pristine PCN-125.

A similar strategy was also applied to HKUST-1 [ $\text{Cu}_3(\text{BTC})_2$ ]<sup>[45]</sup> (Figure 8a),<sup>[36,44]</sup> where the tritopic BTC linkers were partially replaced with ditopic *m*BDC linkers, such as *m*BDC,  $\text{NO}_2$ -*m*BDC, CN-*m*BDC, OH-*m*BDC, 3,5-pyridinedicarboxylate (PDC). To investigate the distribution of defect sites, defect-engineered MOFs (DEMOFs; [ $\text{Cu}_3(\text{BTC})_{(2-x)}$ -(ditopic linker)<sub>*x*</sub>]) were prepared by varying the ratio of the tritopic BTC and ditopic *m*BDC linkers (Figure 8b).<sup>[36]</sup> FT-IR analysis of HKUST-1 indicated that new open metal sites were formed upon addition of ditopic *m*BDC linkers and the degree of defects increased in order of  $\text{NO}_2$ -*m*BDC < CN-*m*BDC < OH-*m*BDC < PDC. Furthermore, it was possible to create mesopores by implementing this defect-engineering strategy. In this case, since the defect sites can change the local structure of the Cu paddle-wheel units, it was expected that the physical properties of such MOFs, including band gap and magnetism, could be finely tuned. Note that removal of the Cu paddle-wheel unit from HKUST-1 can also create defect sites (Figure 8c).<sup>[44]</sup> In this scenario, defective MOFs display greater surface area than their corresponding parent MOF structures.

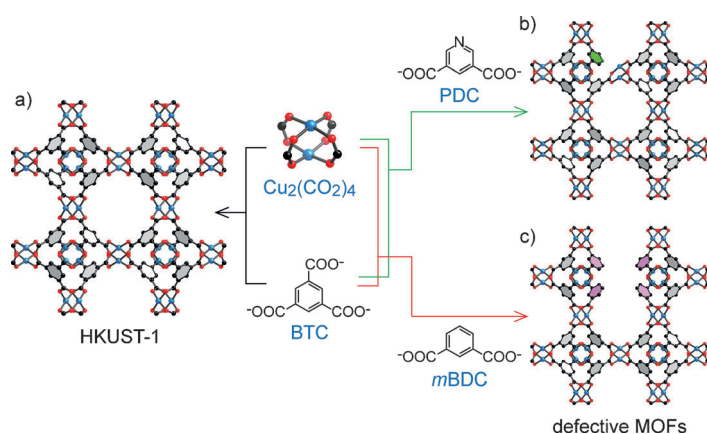


**Figure 8.** A defect-free MOF is composed of Cu paddle-wheels and BTC linkers (a), while defect sites can be introduced by addition of ditopic linkers (b and c). A green benzene ring indicates the ditopic PDC linker and light red benzene rings indicate the *m*BDC linkers.

A recent report showed that it is possible to generate vacancies in MOFs in an ordered manner to produce ordered vacancies. A quarter of the Zn ions and half of the pyrazolecarboxylate (PyC) linkers were removed from a cubic MOF  $[\text{Zn}_4\text{O}(\text{PyC})_3]$  (Figure 9a) to create ordered

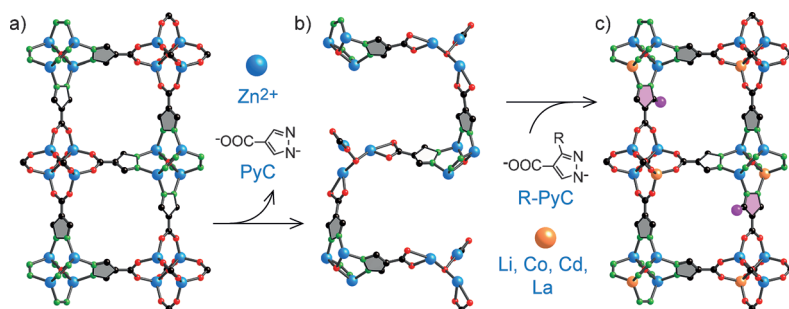


**Figure 9.** By elimination of PyC linkers and metal ions (blue), the single-crystal structure of  $[\text{Zn}_4\text{O}(\text{PyC})_3]$  (a) shows vacancy sites (b). These vacancy sites can be filled again with (functionalized) PyC (pink pyrazole ring) and metal ions (orange) (c).

vacancy sites (i.e. homogeneous MOF in a *srs* topology)  $[\text{Zn}_3\text{O}(\text{OH})(\text{PyC})_{1.5}\text{O}(\text{OH})(\text{H}_2\text{O})_{3.5}(\text{PyC})_{0.5}]$  ( $\square = \text{vacancy}$ ) through single-crystal to single-crystal transformation (Figure 9b).<sup>[46]</sup> After the removal of the metal ions and linkers, rectangular channels appeared, which were of the appropriate size to accommodate large dye molecules (acridine red). This change is remarkable given that no dye inclusion was observed in the pristine MOF samples with no vacancy sites. It is worth noting that these vacancy sites were charge compensated by employing different metal ions (e.g. Li, Co, Cd, and La) and linkers (methyl and amino-functionalized PyC) to rebuild cubic MOF structures (Figure 9c). Such site-directed metal and/or linker replacement was not observed in conventional post-synthetic reactions<sup>[34,35,47,48]</sup> and/or one-pot MOF formation reactions.<sup>[31,33]</sup>

In most cases where MOFs form interpenetrating structures, the connectivity of each framework is identical. However, MOFs with new properties can be achieved by

controlling the level of interpenetration. In 2012, a partially interpenetrated MOF NOTT-202  $\{(\text{Me}_2\text{NH}_2)_{1.75}[\text{In}(\text{BTPC})]_{1.75}\}$  ( $\text{H}_4\text{BTPC} = \text{biphenyl-3,3',5,5'-tetra}(\text{phenyl-4-carboxylic acid})$ ) was synthesized.<sup>[49]</sup> The first net (net A) has a binodal diamondoid topology composed of  $\text{In}^{\text{III}}$  ions and BTPC linkers. The second net (net B) was shown to be two disordered diamond nets, but the occupancy of both nets was 0.375. Therefore, it was concluded that the overall structure could be described as a partially interpenetrating framework (net A:net B = 1:0.75). Interestingly, the  $\text{CO}_2$  isotherm at 195 K of NOTT-202 exhibited a distinctive step with a significant hysteresis loop, whereas at higher temperatures (over 212 K), this step was not observed. The plausible explanation for this is that there was stepwise filling of the pores as a result of structural defect sites generated by the partial interpenetration present.

A final example of complexity in MOFs with interpenetration was unexpectedly observed in MOF-123  $[\text{Zn}_7\text{O}_2(\text{NBD})_5 \cdot (\text{DMF})_2]$  (NBD = 2-nitrobenzene-1,4-dicarboxylate) and its interpenetrating form, MOF-246  $[\text{Zn}_7\text{O}_2(\text{NBD})_5]$ . The reversible interpenetration was triggered through ligand removal and addition.<sup>[50]</sup> The intermediate structure in the interpenetrating process is nearly identical to that in the non-interpenetrating one; nevertheless, gas ( $\text{N}_2$ ,  $\text{CO}_2$ , and  $\text{CH}_4$ ) adsorption behaviors of these materials are different perhaps because of the difference in their local structure.

## 2.6. Mixing of MOFs on Surfaces

As was demonstrated previously, MTV-MOFs can be formed if two or more types of organic linker or metal salt are allowed to react together. Similarly on a MOF surface, a new MOF layer can be formed through sequential MOF formation reactions, especially if the involved MOF structures are similar. Although core-shell type supramolecular structures were reported as early as 2000,<sup>[51]</sup> core-shell MOF structures were not synthesized until 2009.<sup>[48,52]</sup> To prepare core-shell MOF crystals, MOF-5 (IRMOF-3,  $[\text{Zn}_4\text{O}(\text{NH}_2\text{-BDC})_3]$ )<sup>[3b]</sup> seed crystals were synthesized by a conventional solvothermal process and were subsequently immersed in a reaction mixture for IRMOF-3 (MOF-5) to yield core-shell MOFs. By adding this first reaction mixture to the synthesized core-shell MOF crystals, a third layer was formed with microscope images clearly demonstrating the successful MOF coating. Another way to introduce heterogeneity into a MOF structure is by using two different metal ions to form separate MOF domains; this was demonstrated by the preparation of single crystals of  $[\text{Zn}_2(\text{NDC})_2(\text{DABCO})/\text{Cu}_2(\text{NDC})_2(\text{DABCO})]$  (NDC = 1,4-naphthalenedicarboxylate), which contained both Zn and Cu domains.<sup>[52]</sup> However, owing to the small difference in the unit cell length of these two MOFs, synchrotron diffraction analysis revealed that there was rotation of the Cu-MOF lattice by  $11.7^\circ$  with respect to the

Zn-MOF. The crystal interface created by such a rotation angle may have unique properties and applications, such as in molecular filtration and catalysis.

A more practical way to utilize MOF layers, is through the fabrication of thin-layer MOFs.<sup>[53]</sup> An early example of the formation of a MOF thin film (but without heterogeneity) was reported in 2005.<sup>[54]</sup> A thin film of MOF-5 nanocrystals was prepared on carboxylate-terminated self-assembled monolayers (SAMs). This was remarkable as no film was observed to form when bare gold or CF<sub>3</sub>-terminated SAMs were used as substrates. This approach is especially useful for patterning,<sup>[55]</sup> however, AFM images indicate that the surface of the film is not smooth. To mitigate this challenge, step-by-step synthesis of (homogeneous) MOFs was proposed and carried out; copper acetate and BTC linkers were subsequently employed to control the thickness of the resulting MOF film, which was termed as a surface-mounted MOF (SURMOF; Figure 10a).<sup>[56]</sup> The step-by-step growth of this film was confirmed by surface plasmon resonance (SPR) to probe the deposition of MOFs with submonolayer resolution.

More recently, a post-synthetic-modification strategy was implemented to introduce functionalities on the external surface of a SURMOF.<sup>[57]</sup> A SURMOF composed of [Cu<sub>2</sub>-(NDC)<sub>2</sub>(DABCO)] was prepared, followed by surface modification through the addition of NH<sub>2</sub>-BDC to the already formed SURMOF (Figure 10b). Fluorescein isothiocyanate (FITC) was then attached to the NH<sub>2</sub>-functionalized SURMOF through a post-synthetic condensation reaction. The surface-modified SURMOF was grown in both [100] and [001] directions, such that the whole surface of the SURMOF was coated and labeled with NH<sub>2</sub>-BDC and FITC. Furthermore, it was clear that the FITC should only be attached to

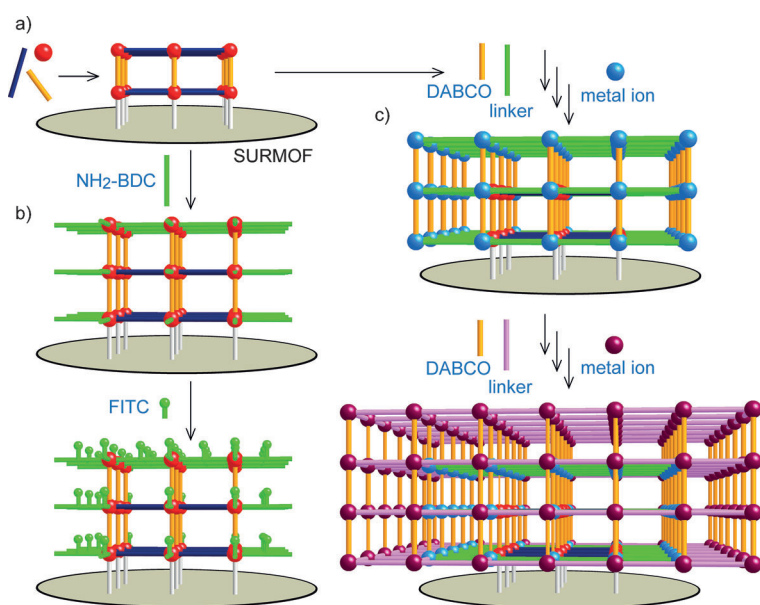


**Figure 10.** Schematic illustration of SURMOF fabrication. a) SURMOFs are prepared on a SAM layer (gray ellipse) by the reaction between metal ions (red sphere) and organic linkers (blue and orange cylinders). b) The surface of the SURMOF can be coated with other organic linkers (green cylinder), and then modified by post synthetic modification reactions. c) Multi-component SURMOFs are also prepared by a reaction of several types of organic linkers and/or metal ions.

the [100] direction, a result of the coordination geometry of the Cu paddle-wheel units. This strategy was then expanded to prepare hybrid SURMOFs, which further enabled the deposition of complex MOF thin films in a controlled manner (Figure 10c).<sup>[57]</sup>

## 2.7. Mixing of Inorganic Materials and MOFs on the Nanoscale

Inorganic nanoparticles coated with MOFs have also been reported. During the early days of research in this area, metal nanoparticles were prepared inside the pores of MOFs by a ship-in-a-bottle approach;<sup>[45,58]</sup> however, it was found to be difficult to control the size of nanoparticles and at the same time increase the loading amount of nanoparticles. Therefore, in recent research, pre-synthesized nanoparticles have been added to the reaction mixture used for MOF syntheses.<sup>[58]</sup> In 2011, gold nanorods were incorporated into [Zn<sub>4</sub>O(BPDC)<sub>3</sub>] microcrystals.<sup>[59]</sup> TEM observations indicate that the nanorods were uniformly dispersed within the MOF structure despite partial aggregation of the nanorods. Enhanced Raman signal provided additional support for the incorporation of these gold nanorods into the MOF framework.

In 2012, nanoparticle-encapsulated ZIF-8 [Zn(CH<sub>3</sub>-Im)<sub>2</sub>]<sup>[20]</sup> nanocrystals were reported.<sup>[60]</sup> By controlling the timing of the addition of polyvinylpyrrolidone (PVP) modified Pt nanoparticles (i.e. beginning of crystal formation or after a certain time, Figure 11), spatial distribution of nanoparticles was precisely controlled. This strategy was also applicable for introducing other PVP-modified nanoparticles, such as CdTe, Fe<sub>3</sub>O<sub>4</sub> nanoparticles, Ag cubes, polystyrene spheres, β-FeOOH rods, and two types of nanoparticles with different diameters. In a similar fashion, Pt nanoparticles were embedded within single crystals of Zr-based MOFs (MOF-801, [Zr<sub>6</sub>O<sub>4</sub>(OH)<sub>4</sub>-(fumarate)<sub>6</sub>]; UiO-66; UiO-67, [Zr<sub>6</sub>O<sub>4</sub>(OH)<sub>4</sub>-(BPDC)<sub>6</sub>]<sup>[61]</sup> with varying pore diameters.<sup>[62]</sup> Hydrogenative methycyclopentane conversion experiments revealed that Zr-MOFs containing Pt nanoparticles (Figure 11 a,h) are able to activate C–C and C–H bonds (to form benzene and cyclohexane) at temperatures approximately 100 °C lower than conventional Pt catalysts. This is in contrast to Pt nanoparticles on nano-sized Zr-MOFs (Figure 11 f,i), which did not yield C<sub>6</sub>-cyclic hydrocarbons.

Several groups reported the incorporation of single metal nanoparticles into nano-sized MOF crystals using different approaches (Figure 11 e).<sup>[63,64]</sup> The first example was the use of pre-synthesized nanocrystals.<sup>[63]</sup> In this method, metal nanocrystals were mixed into a ZIF-8 reaction mixture containing ZIF-8 precursors, which serve as nucleation sites to cover the surface of the nanoparticle with a single crystal of ZIF-8. Interestingly, the (100) planes of the metal particle face the (110) planes of ZIF-8, where it is likely that cetyltrimethylammonium bromide (CTAB)

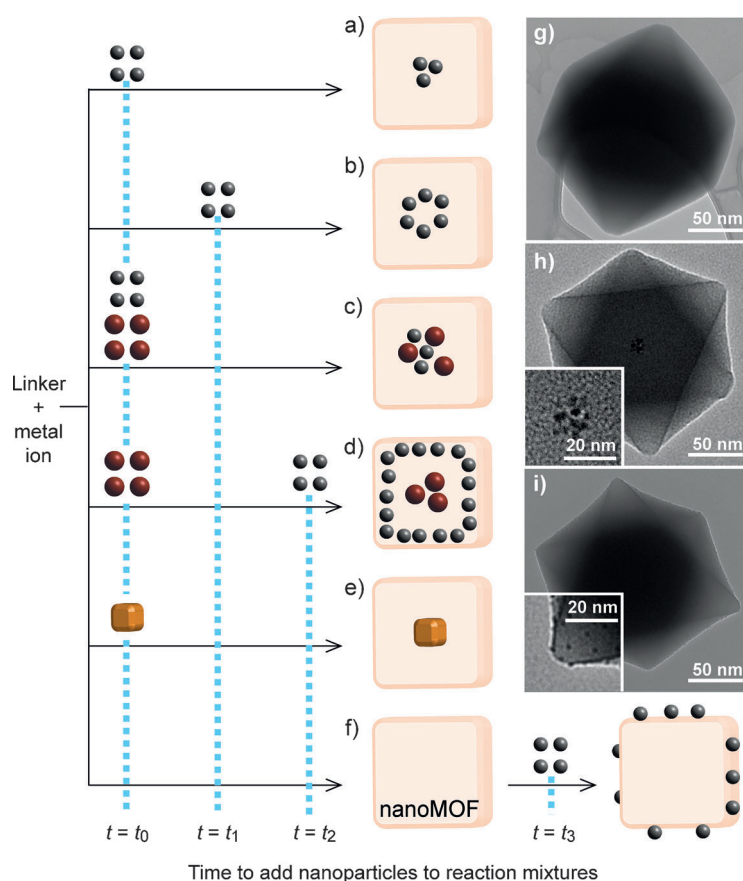


**Figure 11.** a–f) By controlling the timing ( $t_0 < t_1 < t_2 < t_3$ ) for mixing nanoparticles and a reaction mixture of nano-sized MOFs, the spatial distribution of nanoparticles in nano-sized MOFs is controlled. g–i) TEM images of nano-sized UiO-66, Pt containing UiO-66, and UiO-66 whose surface is coated by Pt nanoparticles.

helps to control the alignment between the nanoparticle and ZIF-8.

The second approach reported was a one-pot synthesis to produce MOF-5 containing a single Au nanoparticle<sup>[64]</sup> from a reaction mixture containing  $\text{HAuCl}_4$ ,  $\text{Zn}(\text{NO}_3)_2$ , and  $\text{H}_2\text{BDC}$ . The gold salts were reduced over the course of the reaction, which resulted in Au particles that were coated by MOF-5 (Au@MOF-5) with various thicknesses ( $3.2 \pm 0.5$ ,  $25.1 \pm 4.1$ , and  $69.0 \pm 12.4$  nm). Although the obtained MOF-5 layer was not a single crystal, this method can be widely applicable to synthesize similar core-shell type MOFs with noble metal particles, such as Au@IRMOF-3 and Ag@MOF-5. It is worth noting that only Au@MOF-5 (shell thickness of  $3.2 \pm 0.5$  nm) exhibited an intense surface-enhanced Raman scattering (SERS) signal after exposure to  $\text{N}_2/\text{CO}_2$  (5/1) mixture, whereas other samples (Au@MOF-5 (shell thickness of  $25.1 \pm 4.1$ , and  $69.0 \pm 12.4$  nm), bare Au nanoparticles, and MOF-5 nanoparticles) did not show any SERS signal. Considering that no Raman activity was observed when Au@MOF-5 ( $3.2 \pm 0.5$  nm) was exposed to  $\text{N}_2$ ,  $\text{CO}$ , and  $\text{O}_2$ , it is presumed that adsorbed  $\text{CO}_2$  molecules within the thin-layer of MOF-5 contribute the SERS effects.

## 2.8. MOFs with Heterogeneous Pores

The MOFs described in the previous Section contain nanoparticles within nano-MOF structures; however, there is no void space between the nanoparticles and the MOF nanoparticle. To create extra space, the synthesis of yolk-shell nanostructures was demonstrated in 2012.<sup>[65]</sup> A Pd nanoparticle was coated with a layer of  $\text{Cu}_2\text{O}$ , which was used as a template for the production of a polycrystalline ZIF-8 layer formation with thickness of approximately 100 nm. Interestingly, the majority of the  $\text{Cu}_2\text{O}$  layer was etched off simultaneously during the reaction to create the void space inside the ZIF-8 shell. Note that a ZIF-8 polycrystalline layer was not able to form without clean  $\text{Cu}_2\text{O}$  surface. To create an even larger void space (up to  $5 \mu\text{m}$ ), a spray-drying strategy was also useful.<sup>[66]</sup> In this approach a droplet (i.e. template) of solution containing metal salts and organic linkers is sprayed and then dried. Crystallization of nanocrystals occurs on the surface of the droplet at elevated temperature more readily than conventional solvothermal methods. The product hollow HKUST-1 spheres are stable to mechanical stirring, however the superstructures were degraded to discrete nano-sized MOFs.

In 2012, *meso*-/macroscopic architectures of MOFs were also synthesized.<sup>[67]</sup> An ordered array of  $1 \mu\text{m}$  polystyrene beads was first used as templates to obtain a 3D macroporous metal oxide ( $\text{Al}_2\text{O}_3$ ) architecture, which serves as both a template for a MOF formation reaction as well as a metal source for the MOFs (Figure 12a). When the organic linkers were employed, nano-sized MOF crystals of  $[\text{Al}(\text{OH})(\text{NDC})]^{[68]}$  were formed until the metal source was completely consumed. Consequently, the resulting MOF architectures were nearly identical to the replicated structures of the assembled polystyrene beads. By employing a metal oxide template with different pore structures (e.g. mesoporous alumina aerogel), the entire architectures of MOFs were also controlled. This strategy has is potentially important for optimizing gas/vapor diffusion rates and selectivities in separation processes.

The dimensions of heterogeneous pores in each MOF particle can even reach *meso*- to macro-pore sizes. A unique method was reported to introduce mesoporous domains in MOF-5 materials without losing their crystallinity or porosity (Figure 12b).<sup>[6]</sup> In this work, a controlled amount of 4-(dodecyloxy)benzoic acid (DBA) was added to a reaction mixture of MOF-5, such that a pomegranate-like crystals (pmg-MOF-5, mesopore core and micropore-shell) were obtained. By increasing the amount of DBA, MOF-5 crystals with sponge-like *meso*- and macro-pores were obtained. Although DBA was not found in the activated MOF samples, it is presumed that the alkyl chains of DBA prevent the local crystal growth.

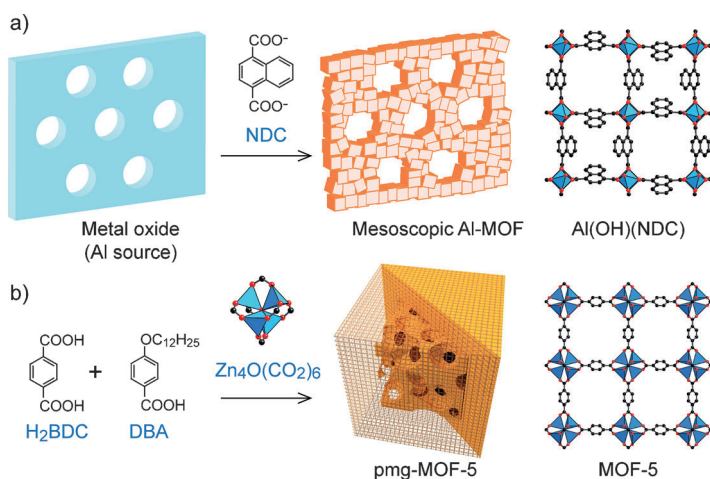


**Figure 12.** a) A mesoscopic MOF architecture is constructed by a replication method.  $\text{Al}_2\text{O}_3$  template (blue plate with large pores) is consumed during the MOF formation, resulting in aggregates of MOF microcrystals. b) pmg-MOF-5 structure is composed of two parts; a *meso*- and *macroporous* core and a *microporous* MOF-5 shell. The original structures of these MOFs are shown on the right.

### 3. MOFs in Industry: An Update

The driving force behind the industrialization of MOFs, as novel solids with hitherto unattainable porosity, is a technology push rather than market pull or society demand. Over the last decade the number of patent applications in industry grew along with the number of MOF structures created in academia which implies the great potential of those materials in various applications (Figure 13).

However, their industrial applicability and economic feasibility are strongly related to their scale-up and therefore production cost. One of the main factors for high costs is multistep organic linkers, therefore the design of organic linkers from inexpensive commodities and backward-integration into carboxylic acids based on renewables will be of importance in the sustainable production of MOFs.

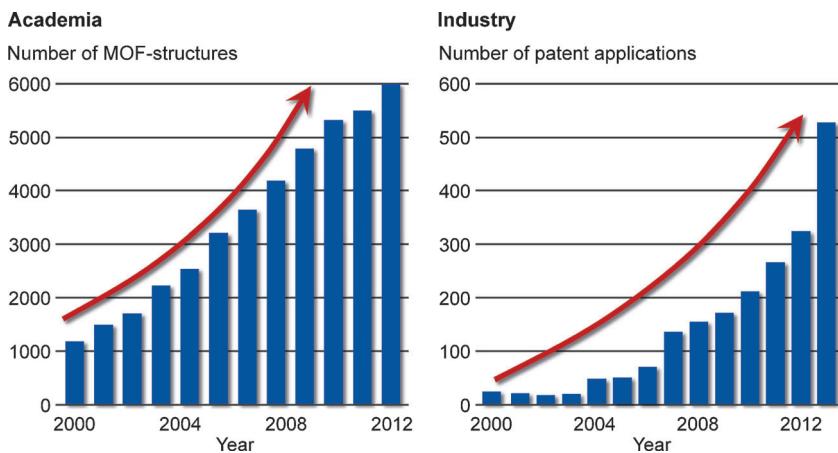


**Figure 13.** A steady increase of patent applications since the year 2000 parallels publications in academia.

MOF synthesis in academia usually is done under solvothermal conditions at elevated temperatures using potentially explosive and corrosive nitrate or chloride salts.<sup>[69]</sup> In industry, safety, health, and environmental (SHE) aspects have to be considered and safer MOF synthesis routes are investigated such as electrochemical syntheses, routes under ambient pressure/conditions or even water-based syntheses. In 2012, BASF received the Pierre Potier Prize for research achievement in the area of MOF synthesis based on a water-borne chemistry in ton scale quantity. The award pays tribute to chemical innovations that support sustainable development. For the same reasons, it is preferable to use non-hazardous metals. Especially for mobile applications lightweight inorganics (e.g. Al and Mg) are preferred over previously used Zn or Cu.

An economic production implies not only the reaction itself and the choice of reactors (batch or continuous) but a carefully designed process including separation of by-products, solvent recycling, waste treatment. Indeed, the overall space-time-yield (STY) (kg of MOF per  $\text{m}^3$  of reaction mixture per day) is regularly used so that the scalability of MOF materials can be easily evaluated.<sup>[69,70]</sup> For optimized MOF syntheses, the STY value is greater than  $5300 \text{ kg m}^{-3} \text{ d}^{-1}$ <sup>[69]</sup> and even up to  $20000 \text{ kg m}^{-3} \text{ d}^{-1}$ , whereas syntheses in academia are usually in the range of  $1\text{--}10 \text{ kg m}^{-3} \text{ d}^{-1}$ . This difference of course is a result of different targets, for example, highly perfect single crystals for structure elucidation or spectroscopy in academia, versus high-rate manufacturing and hence optimized production cost in industry.

In case a volume-limited application is targeted, for example, mobile natural-gas storage for automotive use, improvements in volume-specific density are a must. Typically the manufacturing chain from a powder of MOF into an industrially optimized shaped body easily requires a densification of a about a factor of 2–3. In general, there are two ways to make shaped bodies,<sup>[71]</sup> namely dry compacting into pellets or granulates or extrusion into strands by an aqueous process. Generally binders and lubricants are used in both processes to reach optimum mechanical stability needed for the later on application.

Prior to shaping of powders, computational methods, for example, computational fluid dynamics (CFD) are applied to simulate optimized particle and packing geometry, tortuosity, heat and mass transfer properties.

Owing to their high porosity, well-defined structure, and architectural stability, MOFs have high potential for industrial applications, including gas separation, gas storage, catalysis, sensors, electronics, optics, medical use and water treatment. Out of these fields adsorption is now close to market entry (Figure 14).

BASF is focused on commercializing MOF solutions for the transportation

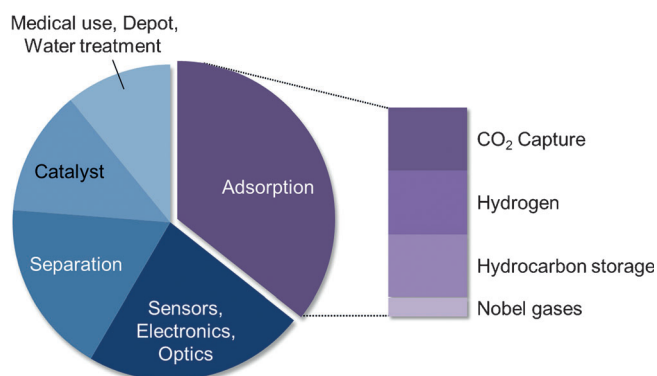


Figure 14. Patents claiming various fields of industrial use.

industry. BASF is partnering with several technology, development and original-equipment manufacturers (OEMs) to pilot the use of MOF materials for enhanced natural-gas storage in vehicles in Europe, Asia, and North America.

Demonstration vehicles equipped with natural-gas fuel systems containing BASF MOF materials were introduced in 2012, including light (FIAT, Volkswagen) and heavy duty (Kenworth) vehicles. The up-fitted BASF-Car fleet proved BASF's energy storage technology to be a viable technology with several ten thousands of test kilometers (Figure 15).



Figure 15. Viable technology for mobile natural-gas storage at BASF (from left Dr. F. Seitz, Dr. U. Müller, Dr. S. Maurer, Dr. L. Arnold, Prof. Dr. O. Yaghi, Dr. S. Marx).

#### 4. Summary and Outlook

The different forms of heterogeneity presented above are all superimposed onto an otherwise metrically and compositionally well-defined MOF structure. Since in most cases the elements giving rise to heterogeneity are either covalently linked to the ordered structure or encompassed by it, it might be possible to organize these elements in various patterns, sequences, and regions to code for specific properties. The fact that the heterogeneity is metrically defined (the distances between the heterogeneous elements is fixed and can be determined from the MOF backbone structure) will eventually allow characterization of the heterogeneity and its correlation to function. It is worth noting, that when post-synthetic modification<sup>[47]</sup> is carried out on a MOF, unless the reaction is quantitative, this system falls within the realm of

building 'heterogeneity within order' because unreacted linker functionalities remain as an integral part of the MOF and indeed make the pore environment chemically heterogeneous. With this observation and the points outlined in this Review, the science of heterogeneity in MOFs raises new questions, which require new methods and perhaps characterization tools for studying MOF chemistry. Concerning the industry of MOFs, BASF efforts clearly show that MOFs are poised to enter the marketplace for methane storage in automobile fuel tanks.

We acknowledge Dr. Lena Arnold and Dr. Alex U. Czaja (BASF SE) for discussions of MOFs in industry, and Mr. K. E. Cordova and Dr. K. M. Choi (Yaghi group) for their valuable input. Financial support for MOF research in O.M.Y. laboratories is provided by BASF SE (Ludwigshafen, Germany); U.S. Department of Energy, Office of Science, Office of Basic Energy Sciences, Energy Frontier Research Center grant DE-SC0001015; U.S. Department of Defense, Defense Threat Reduction Agency grant HDTRA 1-12-1-0053, and King Abdulaziz City of Science and Technology, Riyadh, Saudi Arabia.

Received: October 19, 2014

Published online: January 13, 2015

- [1] a) O. M. Yaghi, G. Li, H. Li, *Nature* **1995**, 378, 703–706; b) H. Li, M. Eddaoudi, T. L. Groy, O. M. Yaghi, *J. Am. Chem. Soc.* **1998**, 120, 8571–8572; c) O. M. Yaghi, H. Li, C. Davis, D. Richardson, T. L. Groy, *Acc. Chem. Res.* **1998**, 31, 474–484.
- [2] a) U. Mueller, M. Schubert, F. Teich, H. Puetter, K. Schierle-Arndt, J. Pastré, *J. Mater. Chem.* **2006**, 16, 626–636; b) M. Jacoby, *Chem. Eng. News* **2008**, 86, 13–16.
- [3] a) J. S. Seo, D. Whang, H. Lee, S. I. Jun, J. Oh, Y. J. Jeon, K. Kim, *Nature* **2000**, 404, 982–986; b) M. Eddaoudi, J. Kim, N. L. Rosi, D. T. Vodak, J. Wachter, M. O'Keeffe, O. M. Yaghi, *Science* **2002**, 295, 469–472; c) H. K. Chae, D. Y. Siberio-Perez, J. Kim, Y.-B. Go, M. Eddaoudi, A. J. Matzger, M. O'Keeffe, O. M. Yaghi, *Nature* **2004**, 427, 523–527; d) G. Férey, C. Mellot-Draznieks, C. Serre, F. Millange, J. Dutour, S. Surblé, I. Margiolaki, *Science* **2005**, 309, 2040–2042; e) J. A. Hurd, R. Vaidhyanathan, V. Thangadurai, C. I. Ratcliffe, I. L. Moudrakovski, G. K. H. Shimizu, *Nat. Chem.* **2009**, 1, 705–710; f) P. Küsgens, M. Rose, I. Senkowska, H. Fröde, A. Henschel, S. Siegle, S. Kaskel, *Microporous Mesoporous Mater.* **2009**, 120, 325–330; g) O. K. Farha, A. O. Yazaydin, I. Eryazici, C. D. Malliakas, B. G. Hauser, M. G. Kanatzidis, S.-B. T. Nguyen, R. Q. Snurr, J. T. Hupp, *Nat. Chem.* **2010**, 2, 944–948; h) E. D. Bloch, W. L. Queen, R. Krishna, J. M. Zadrozny, C. M. Brown, J. R. Long, *Science* **2012**, 335, 1606–1610; i) C. Wang, K. E. deKrafft, W. Lin, *J. Am. Chem. Soc.* **2012**, 134, 7211–7214; j) R. F. D'Vries, V. A. de La Peña-O'Shea, N. Snejko, M. Iglesias, E. Gutiérrez-Puebla, M. A. Monge, *J. Am. Chem. Soc.* **2013**, 135, 5782–5792; k) A. Foucault-Collet, K. A. Gogick, K. A. White, S. Villette, A. Pallier, G. Collet, C. Kieda, T. Li, S. J. Geib, N. L. Rosi, S. Petoud, *Proc. Natl. Acad. Sci. USA* **2013**, 110, 17199–17204; l) F. M. Hinterholzinger, B. Rühle, S. Wuttke, K. Karaghiosoff, T. Bein, *Sci. Rep.* **2013**, 3, 2562-1–2562-7; m) V. Guillerme, Ł. J. Weseliński, Y. Belmabkhout, A. J. Cairns, V. D'Elia, Ł. Wojtas, K. Adil, M. Eddaoudi, *Nat. Chem.* **2014**, 6, 673–680; n) B. Li, H.-M. Wen, H. Wang, H. Wu, M. Tyagi, T. Yildirim, W. Zhou, B. Chen, *J. Am. Chem. Soc.* **2014**, 136, 6207–6210.

- [4] a) O. M. Yaghi, M. O’Keeffe, N. W. Ockwig, H. K. Chae, M. Eddaoudi, J. Kim, *Nature* **2003**, *423*, 705–714; b) S. Kitagawa, R. Kitaura, S. Noro, *Angew. Chem. Int. Ed.* **2004**, *43*, 2334–2375; *Angew. Chem.* **2004**, *116*, 2388–2430; c) H. Wu, Q. Gong, D. H. Olson, J. Li, *Chem. Rev.* **2012**, *112*, 836–868; d) J.-P. Zhang, Y.-B. Zhang, J.-B. Lin, X.-M. Chen, *Chem. Rev.* **2012**, *112*, 1001–1033; e) H. Furukawa, K. E. Cordova, M. O’Keeffe, O. M. Yaghi, *Science* **2013**, *341*, 974; f) J. A. Mason, M. Veenstra, J. R. Long, *Chem. Sci.* **2014**, *5*, 32–51.
- [5] a) D. N. Bunck, W. R. Dichtel, *Chem. Eur. J.* **2013**, *19*, 818–827; b) A. B. Cairns, A. L. Goodwin, *Chem. Soc. Rev.* **2013**, *42*, 4881–4893.
- [6] K. M. Choi, H. J. Jeon, J. K. Kang, O. M. Yaghi, *J. Am. Chem. Soc.* **2011**, *133*, 11920–11923.
- [7] H. Deng, C. J. Doonan, H. Furukawa, R. B. Ferreira, J. Towne, C. B. Knobler, B. Wang, O. M. Yaghi, *Science* **2010**, *327*, 846–850.
- [8] X. Kong, H. Deng, F. Yan, J. Kim, J. A. Swisher, B. Smit, O. M. Yaghi, J. A. Reimer, *Science* **2013**, *341*, 882–885.
- [9] K. Seki, *Chem. Commun.* **2001**, 1496–1497.
- [10] a) B.-Q. Ma, K. L. Mulfort, J. T. Hupp, *Inorg. Chem.* **2005**, *44*, 4912–4914; b) R. Kitaura, F. Iwahori, R. Matsuda, S. Kitagawa, Y. Kubota, M. Takata, T. C. Kobayashi, *Inorg. Chem.* **2004**, *43*, 6522–6524; c) D. N. Dybtsev, H. Chun, K. Kim, *Angew. Chem. Int. Ed.* **2004**, *43*, 5033–5036; *Angew. Chem.* **2004**, *116*, 5143–5146; d) R. Wang, L. Han, F. Jiang, Y. Zhou, D. Yuan, M. Hong, *Cryst. Growth Des.* **2005**, *5*, 129–135; e) S. Dalai, P. S. Mukherjee, E. Zangrando, F. Lloret, N. R. Chaudhuri, *J. Chem. Soc. Dalton Trans.* **2002**, 822–823; f) S. W. Lee, H. J. Kim, Y. K. Lee, K. Park, J.-H. Son, Y.-U. Kwon, *Inorg. Chim. Acta* **2003**, *353*, 151–158.
- [11] a) The topology of MOFs is typically represented with a three-letter code; M. O’Keeffe, M. A. Peskov, S. J. Ramsden, O. M. Yaghi, *Acc. Chem. Res.* **2008**, *41*, 1782–1789; b) O. Delgado-Friedrichs, M. O’Keeffe, O. M. Yaghi, *Phys. Chem. Chem. Phys.* **2007**, *9*, 1035–1043.
- [12] a) K. Koh, A. G. Wong-Foy, A. J. Matzger, *Angew. Chem. Int. Ed.* **2008**, *47*, 677–680; *Angew. Chem.* **2008**, *120*, 689–692; b) K. Koh, A. G. Wong-Foy, A. J. Matzger, *J. Am. Chem. Soc.* **2009**, *131*, 4184–4185.
- [13] H. Furukawa, N. Ko, Y. B. Go, N. Aratani, S. B. Choi, E. Choi, A. Ö. Yazaydin, R. Q. Snurr, M. O’Keeffe, J. Kim, O. M. Yaghi, *Science* **2010**, *329*, 424–428.
- [14] a) L. Liu, K. Konstas, M. R. Hill, S. G. Telfer, *J. Am. Chem. Soc.* **2013**, *135*, 17731–17734; b) A. Dutta, A. G. Wong-Foy, A. J. Matzger, *Chem. Sci.* **2014**, *5*, 3729–3734.
- [15] a) R. Banerjee, A. Phan, B. Wang, C. Knobler, H. Furukawa, M. O’Keeffe, O. M. Yaghi, *Science* **2008**, *319*, 939–943; b) A. Phan, C. J. Doonan, F. J. Uribe-Romo, C. B. Knobler, M. O’Keeffe, O. M. Yaghi, *Acc. Chem. Res.* **2010**, *43*, 58–67; c) T. Wu, X. Bu, J. Zhang, P. Feng, *Chem. Mater.* **2008**, *20*, 7377–7382.
- [16] R. Banerjee, H. Furukawa, D. Britt, C. Knobler, M. O’Keeffe, O. M. Yaghi, *J. Am. Chem. Soc.* **2009**, *131*, 3875–3877.
- [17] N. T. T. Nguyen, H. Furukawa, F. Gándara, H. T. Nguyen, K. E. Cordova, O. M. Yaghi, *Angew. Chem. Int. Ed.* **2014**, *53*, 10645–10648; *Angew. Chem.* **2014**, *126*, 10821–10824.
- [18] a) D. J. Tranchemontagne, J. L. Mendoza-Cortes, M. O’Keeffe, O. M. Yaghi, *Chem. Soc. Rev.* **2009**, *38*, 1257–1283; b) M. Li, D. Li, M. O’Keeffe, O. M. Yaghi, *Chem. Rev.* **2014**, *114*, 1343–1370.
- [19] B. Zhao, P. Cheng, Y. Dai, C. Cheng, D.-Z. Liao, S.-P. Yan, Z.-H. Jiang, G.-L. Wang, *Angew. Chem. Int. Ed.* **2003**, *42*, 934–936; *Angew. Chem.* **2003**, *115*, 964–966.
- [20] K. S. Park, Z. Ni, A. P. Côté, J. Y. Choi, R. Huang, F. J. Uribe-Romo, H. K. Chae, M. O’Keeffe, O. M. Yaghi, *Proc. Natl. Acad. Sci. USA* **2006**, *103*, 10186–10191.
- [21] Z. Wang, V. C. Kravtsov, M. J. Zaworotko, *Angew. Chem. Int. Ed.* **2005**, *44*, 2877–2880; *Angew. Chem.* **2005**, *117*, 2937–2940.
- [22] A. G. Wong-Foy, O. Lebel, A. J. Matzger, *J. Am. Chem. Soc.* **2007**, *129*, 15740–15741.
- [23] X. Zhao, X. Wang, J. Dou, P. Cui, Z. Chen, D. Sun, X. Wang, D. Sun, *Cryst. Growth Des.* **2012**, *12*, 2736–2739.
- [24] F. Nouar, J. F. Eubank, T. Bousquet, L. Wojtas, M. J. Zaworotko, M. Eddaoudi, *J. Am. Chem. Soc.* **2008**, *130*, 1833–1835.
- [25] M. Eddaoudi, J. Kim, J. B. Wachter, H. K. Chae, M. O’Keeffe, O. M. Yaghi, *J. Am. Chem. Soc.* **2001**, *123*, 4368–4369.
- [26] S.-T. Zheng, T. Wu, B. Irfanoglu, F. Zuo, P. Feng, X. Bu, *Angew. Chem. Int. Ed.* **2011**, *50*, 8034–8037; *Angew. Chem.* **2011**, *123*, 8184–8187.
- [27] A. Schoedel, A. J. Cairns, Y. Belmabkhout, L. Wojtas, M. Mohamed, Z. Zhang, D. M. Proserpio, M. Eddaoudi, M. J. Zaworotko, *Angew. Chem. Int. Ed.* **2013**, *52*, 2902–2905; *Angew. Chem.* **2013**, *125*, 2974–2977.
- [28] H. Li, M. Eddaoudi, M. O’Keeffe, O. M. Yaghi, *Nature* **1999**, *402*, 276–279.
- [29] T.-H. Park, K. Koh, A. G. Wong-Foy, A. J. Matzger, *Cryst. Growth Des.* **2011**, *11*, 2059–2063.
- [30] H. Tamaki, Z. J. Zhong, N. Matsumoto, S. Kida, M. Koikawa, N. Achiwa, Y. Hashimoto, H. Okawa, *J. Am. Chem. Soc.* **1992**, *114*, 6974–6979.
- [31] J. A. Botas, G. Calleja, M. Sánchez-Sánchez, M. G. Orcajo, *Langmuir* **2010**, *26*, 5300–5303.
- [32] N. L. Rosi, J. Kim, B. Chen, M. Eddaoudi, M. O’Keeffe, O. M. Yaghi, *J. Am. Chem. Soc.* **2005**, *127*, 1504–1518.
- [33] L. J. Wang, H. Deng, H. Furukawa, F. Gándara, K. E. Cordova, D. Peri, O. M. Yaghi, *Inorg. Chem.* **2014**, *53*, 5881–5883.
- [34] S. Das, H. Kim, K. Kim, *J. Am. Chem. Soc.* **2009**, *131*, 3814–3815.
- [35] C. K. Brozek, M. Dincă, *J. Am. Chem. Soc.* **2013**, *135*, 12886–12891.
- [36] Z. Fang, J. P. Dürholt, M. Kauer, W. Zhang, C. Lochenie, B. Jee, B. Albada, N. Metzler-Nolte, A. Pöpl, B. Weber, M. Muhler, Y. Wang, R. Schmid, R. A. Fischer, *J. Am. Chem. Soc.* **2014**, *136*, 9627–9636.
- [37] F. Vermoortele, R. Ameloot, L. Alaerts, R. Mattheessen, B. Carlier, E. V. R. Fernandez, J. Gascon, F. Kapteijn, D. E. De Vos, *J. Mater. Chem.* **2012**, *22*, 10313–10321.
- [38] M. J. Ingleson, J. P. Barrio, J. Bacsá, C. Dickinson, H. Park, M. J. Rosseinsky, *Chem. Commun.* **2008**, 1287–1289.
- [39] F. Vermoortele, B. Bueken, G. Le Bars, B. Van de Voorde, M. Vandichel, K. Houthoofd, A. Vimont, M. Daturi, M. Waroquier, V. Van Speybroeck, C. Kirschhock, D. E. De Vos, *J. Am. Chem. Soc.* **2013**, *135*, 11465–11468.
- [40] a) H. Wu, Y. S. Chua, V. Krungleviciute, M. Tyagi, P. Chen, T. Yildirim, W. Zhou, *J. Am. Chem. Soc.* **2013**, *135*, 10525–10532; b) M. J. Cliffe, W. Wan, X. Zou, P. A. Chater, A. K. Kleppe, M. G. Tucker, H. Wilhelm, N. P. Funnell, F.-X. Coudert, A. L. Goodwin, *Nat. Commun.* **2014**, *5*, 4176.
- [41] U. Ravon, M. Savonnet, S. Aguado, M. E. Domine, E. Janneau, D. Farrusseng, *Microporous Mesoporous Mater.* **2010**, *129*, 319–329.
- [42] L. Huang, H. Wang, J. Chen, Z. Wang, J. Sun, D. Zhao, Y. Yan, *Microporous Mesoporous Mater.* **2003**, *58*, 105–114.
- [43] J. Park, Z. U. Wang, L.-B. Sun, Y.-P. Chen, H.-C. Zhou, *J. Am. Chem. Soc.* **2012**, *134*, 20110–20116.
- [44] G. Barin, V. Krungleviciute, O. Gutov, J. T. Hupp, T. Yildirim, O. K. Farha, *Inorg. Chem.* **2014**, *53*, 6914–6919.
- [45] S. S.-Y. Chui, S. M.-F. Lo, J. P. H. Charmant, A. G. Orpen, I. D. Williams, *Science* **1999**, *283*, 1148–1150.
- [46] B. Tu, Q. Pang, D. Wu, Y. Song, L. Weng, Q. Li, *J. Am. Chem. Soc.* **2014**, *136*, 14465–14471.
- [47] S. M. Cohen, *Chem. Rev.* **2012**, *112*, 970–1000.
- [48] K. Koh, A. G. Wong-Foy, A. J. Matzger, *Chem. Commun.* **2009**, 6162–6164.
- [49] S. Yang, X. Lin, W. Lewis, M. Suyetin, E. Bichoutskaia, J. E. Parker, C. C. Tang, D. R. Allan, P. J. Rizkallah, P. Hubberstey,

- N. R. Champness, K. M. Thomas, A. J. Blake, M. Schröder, *Nat. Mater.* **2012**, *11*, 710–716.
- [50] S. B. Choi, H. Furukawa, H. J. Nam, D. Y. Jung, Y. H. Jhon, A. Walton, D. Book, M. O’Keeffe, O. M. Yaghi, J. Kim, *Angew. Chem. Int. Ed.* **2012**, *51*, 8791–8795; *Angew. Chem.* **2012**, *124*, 8921–8925.
- [51] J. C. MacDonald, P. C. Dorrestein, M. M. Pilley, M. M. Foote, J. L. Lundburg, R. W. Henning, A. J. Schultz, J. L. Manson, *J. Am. Chem. Soc.* **2000**, *122*, 11692–11702.
- [52] S. Furukawa, K. Hirai, K. Nakagawa, Y. Takashima, R. Matsuda, T. Tsuruoka, M. Kondo, R. Haruki, D. Tanaka, H. Sakamoto, S. Shimomura, O. Sakata, S. Kitagawa, *Angew. Chem. Int. Ed.* **2009**, *48*, 1766–1770; *Angew. Chem.* **2009**, *121*, 1798–1802.
- [53] a) O. Shekhah, J. Liu, R. A. Fischer, C. Wöll, *Chem. Soc. Rev.* **2011**, *40*, 1081–1106; b) A. Bétard, R. A. Fischer, *Chem. Rev.* **2012**, *112*, 1055–1083.
- [54] S. Hermes, F. Schroder, R. Chelmoski, C. Wöll, R. A. Fischer, *J. Am. Chem. Soc.* **2005**, *127*, 13744–13745.
- [55] G. Lu, O. K. Farha, W. Zhang, F. Huo, J. T. Hupp, *Adv. Mater.* **2012**, *24*, 3970–3974.
- [56] O. Shekhah, H. Wang, S. Kowarik, F. Schreiber, M. Paulus, M. Tolan, C. Sternemann, F. Evers, D. Zacher, R. A. Fischer, C. Wöll, *J. Am. Chem. Soc.* **2007**, *129*, 15118–15119.
- [57] a) B. Liu, M. Ma, D. Zacher, A. Bétard, K. Yusenko, N. Metzler-Nolte, C. Wöll, R. A. Fischer, *J. Am. Chem. Soc.* **2011**, *133*, 1734–1737; b) D. Zacher, K. Yusenko, A. Bétard, S. Henke, M. Molon, T. Ladnorg, O. Shekhah, B. Schüpbach, T. de Los Arcos, M. Krasnopolski, M. Meilikhov, J. Winter, A. Terfort, C. Wöll, R. A. Fischer, *Chem. Eur. J.* **2011**, *17*, 1448–1455; c) B. Liu, M. Tu, D. Zacher, R. A. Fischer, *Adv. Funct. Mater.* **2013**, *23*, 3790–3798.
- [58] Q.-L. Zhu, Q. Xu, *Chem. Soc. Rev.* **2014**, *43*, 5468–5512.
- [59] K. Sugikawa, Y. Furukawa, K. Sada, *Chem. Mater.* **2011**, *23*, 3132–3134.
- [60] G. Lu, S. Li, Z. Guo, O. K. Farha, B. G. Hauser, X. Qi, Y. Wang, X. Wang, S. Han, X. Liu, J. S. DuChene, H. Zhang, Q. Zhang, X. Chen, J. Ma, S. C. J. Loo, W. D. Wei, Y. Yang, J. T. Hupp, F. Huo, *Nat. Chem.* **2012**, *4*, 310–316.
- [61] a) J. H. Cavka, S. Jakobsen, U. Olsbye, N. Guillou, C. Lamberti, S. Bordiga, K. P. Lillerud, *J. Am. Chem. Soc.* **2008**, *130*, 13850–13851; b) G. Wißmann, A. Schaate, S. Lilienthal, I. Bremer, A. Schneider, P. Behrens, *Microporous Mesoporous Mater.* **2012**, *152*, 64–70; c) H. Furukawa, F. Gándara, Y.-B. Zhang, J. Jiang, W. L. Queen, M. R. Hudson, O. M. Yaghi, *J. Am. Chem. Soc.* **2014**, *136*, 4369–4381.
- [62] K. Na, K. M. Choi, O. M. Yaghi, G. A. Somorjai, *Nano Lett.* **2014**, *14*, 5979–5983.
- [63] P. Hu, J. Zhuang, L.-Y. Chou, H. K. Lee, X. Y. Ling, Y.-C. Chuang, C.-K. Tsung, *J. Am. Chem. Soc.* **2014**, *136*, 10561–10564.
- [64] L. He, Y. Liu, J. Liu, Y. Xiong, J. Zheng, Y. Liu, Z. Tang, *Angew. Chem. Int. Ed.* **2013**, *52*, 3741–3745; *Angew. Chem.* **2013**, *125*, 3829–3833.
- [65] C.-H. Kuo, Y. Tang, L.-Y. Chou, B. T. Sneed, C. N. Brodsky, Z. Zhao, C.-K. Tsung, *J. Am. Chem. Soc.* **2012**, *134*, 14345–14348.
- [66] A. Carné-Sánchez, I. Imaz, M. Cano-Sarabia, D. Maspocho, *Nat. Chem.* **2013**, *5*, 203–211.
- [67] J. Reboul, S. Furukawa, N. Horike, M. Tsotsalas, K. Hirai, H. Uehara, M. Kondo, N. Louvain, O. Sakata, S. Kitagawa, *Nat. Mater.* **2012**, *11*, 717–723.
- [68] A. Comotti, S. Bracco, P. Sozzani, S. Horike, R. Matsuda, J. Chen, M. Takata, Y. Kubota, S. Kitagawa, *J. Am. Chem. Soc.* **2008**, *130*, 13664–13672.
- [69] B. Yilmaz, N. Trukhan, U. Müller, *Chin. J. Catal.* **2012**, *33*, 3–10.
- [70] A. U. Czaja, N. Trukhan, U. Müller, *Chem. Soc. Rev.* **2009**, *38*, 1284–1293.
- [71] M. Hesse, U. Mueller, O. M. Yaghi, US patent 7,524,444 B2, **2009**.